Preparation of Antibacterial and Strong Regenerated Cellulose Film *via* Crosslinking with Polymeric Quaternary Ammonium Salt Containing Epoxy/ZnO

Meng Zhang, Xiaoning Tang, Tian Si,* Xueping Wang, and Xue Wu

**Corresponding author: jayzhou-@163.com*

DOI: 10.15376/biores.19.2.2149-2159

GRAPHICAL ABSTRACT

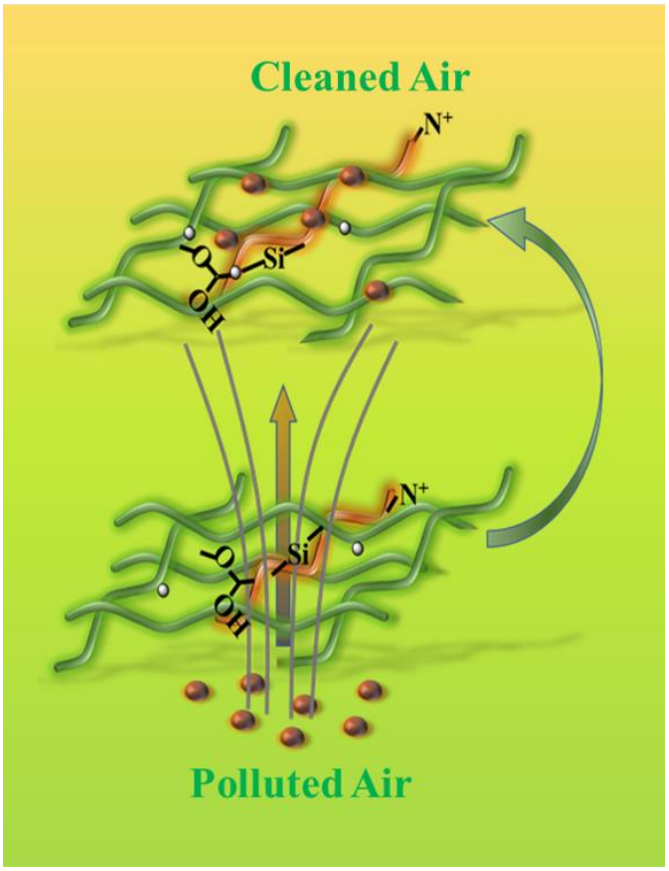

Preparation of Antibacterial and Strong Regenerated Cellulose Film *via* Crosslinking with Polymeric Quaternary Ammonium Salt Containing Epoxy/ZnO

Meng Zhang, Xiaoning Tang, Tian Si,* Xueping Wang, and Xue Wu

Particulate matter (PM), usually formed as aerosols suspended in atmosphere, is becoming a carrier of viruses and bacteria, accelerating the spread of respiratory diseases. Hence, air filtration devices are widely utilized for removing PM. In this study, a regenerated cellulose (RC) film was prepared with the properties of good mechanical strength, antibacterial, and highly efficient filtration (EF) properties, through cellulose dissolution and further crosslinking with P(AGE-DMDAAC)/ZnO. Results exhibited that the Young's modulus of the composite membrane was nearly 4.3 GPa. Additionally, the antibacterial performance against *Escherichia coli* and *Staphylococcus aureus*, was up to 99.89% and 99.67%, respectively. Meanwhile, RC composite filter exhibited a high PM 2.5 capture efficiency (over 99.91%). This study introduces an interesting approach to produce antibacterial films with the characteristics of notably good mechanical performance and high fine particle EF that can be utilized in a high humidity environment.

DOI: 10.15376/biores.19.2.2149-2159

Keywords: Regenerated cellulose; Cellulose cross-linking; Antimicrobial films

*Contact information: Faculty of Chemical Engineering, Kunming University of Science and Technology, Kunming 650500, Yunnan, China; *Corresponding author: jayzhou-@163.com*

INTRODUCTION

In recent decades, with the rapid development of industrialization and urbanization in human society, air pollution has become increasingly prominent and has attracted increased attention worldwide (Zhu *et al*. 2017). Particulate matter (PM) is one of the major air pollutants generated with human activities, leading to the damage of bronchi and lungs (Salama *et al*. 2021). Industrial emissions, vehicle exhaust, and even crop burning release large amounts of PMx. Hence, air filters are widely applied for the capture of biological particles and their aerosols due to their high particle removal efficiency (Hartikainen *et al*. 2001). However, the bacteria enriched in air filters can be still alive, leading to a secondary pollution (Holdsworth and Law 2012). Therefore, the design of a novel air filtration device should also consider their antimicrobial capabilities.

Billions of tons of crop straw are grown each year in China, but the utilization rate is usually only nearly 15%. Corn stalks can be divided into fibre cells and parenchyma cells. Parenchyma cells are characterized as large specific surface area, soft texture, low crystallinity, and ability of store nutrients. In terms of the accessibility and reactivity of chemical reagents, the parenchymal cellulose is superior. Due to its stable structure, environmental friendliness, low biological toxicity, and strong plasticity, regenerated cellulose (RC) has attracted widespread attention (Mir *et al*. 2016). However, limited by

its unique semi-crystalline structure, the strength of materials consisted of RC is usually relatively poor compared with fossil-based polymers (Shatkin *et al*. 2014). Therefore, the mechanical properties of cellulosic films can be effectively improved through composite formation with other polymers. Nanocomposite membranes prepared from organic substrates (NC-PVA) have mechanical advantages for industrial applications. Pure NC composites exhibited the highest storage modulus and thermal stability (Poyraz *et al*. 2017). Cellulose has been applied widely such as paper making, medical, and packaging, *etc*., on account of its properties of degradability, low toxicity, and low cost (Candan *et al*. 2022).

Dimethyldiallylammonium chloride (DMDAAC) has been widely used as a water-soluble cationic monomer, taking advantage of its highly active double bonds to take part in free-radical initiated addition polymerization. When an epoxy group of allyl glycidyl ester (AGE) is introduced into DMDAAC polymer, the properties of antibacterial and mechanical strength were enhanced. Hence, authors expected good results using DMDAAC as a reinforcing material with RC (Ren *et al*. 2008).

DMDAAC is easy to produce resistance and other shortcomings, as a quaternary ammonium salt fungicide. By combining it with polymer materials, the mechanical weakness of cellulose was improved notably. In this study, P(AGE-DMDAAC)/ZnO was prepared through a simple and facile *in-situ* polymerization method based on RC from corn stalk parenchyma. The results suggested that a net-like structure was obtained due to the addition of P/ZnO, which remarkably improved the strength of RC films.

EXPERIMENTAL

Materials

The corn stover was obtained from Yuxi area in Yunnan province, China. Zinc chloride ($ZnCl_2$, 95%) and sodium hydroxide (NaOH, 99%) were purchased from Tianjin Fengchuan Chemical Reagent Technologies Co., Ltd. (China). Diallyl dimethyl ammonium chloride (DMDAAC, 60%), potassium peroxydisulfate (KPS), methylacryloxy propyl trimethoxy silane (KH-570), and allyl glycidyl ether (AGE) were purchased from Aladdin Chemical Reagent Co. Ltd. Trypsin, and agar were sourced from Aobox Biotechnology Company (Beijing, China).

Cellulose preparation

Corn stalks were air-dried, peeled, and powdered. 15 g of straw powder was put into 600 mL deionized (DI) water. After that, 12.6 g sodium chlorite and 7.5 mL glacial acetic acid was added. Heating in a water bath was done at 85 ℃ for 1 hour, then 6 g sodium chloride and 4 mL glacial acetic acid were repeatedly added for 7 times to obtain the holocellulose. The hemicellulose was distributed with DI water (solid-liquid ratio was 1:20) and 10% (w/v) potassium hydroxide (KOH).

Preparation of nano ZnO

The pH of $ZnCl_2$ solution (60 ℃) was controlled at 11.0 with NaOH solution, with stirring at 400 rpm. The mixture was precipitated by a centrifugation process, washed 4 times with deionized water, and kept at 400 ℃ for 2 h in an oven to form a nano-ZnO.

Synthesis of P(AGE-DMDAAC)/ZnO

Various amounts of nano ZnO (0.024 g, 0.071 g, 0.119 g, 0.166 g, 0.238 g, *etc*.) were dispersed in 7.5 g of water. Then, a silane coupling agent KH-570 (0.90 g) and DMDAAC (23.75 g) were added into the mixture. The mixture was treated in an ultrasonic mixer with ice-water bath under nitrogen atmosphere for at least 30 min. Then, desired quantities of KPS (1.19 g, 2.38 g, 3.56 g, 4.75 g, 5.94 g) and allyl glycidyl ether (370 µL) were added into the mixture and stirred at 400 rpm under 80 ℃ for 4 h. P(AGE-DMDAAC)/ZnO is abbreviated as P/ZnO in the following text.

Preparation of RC/P/ZnO composite film

The freeze-dried cellulose raw material was dissolved in 6% DMAc/LiCl system, and then P/ZnO (The mass ratio of P/ZnO to cellulose was 1:10) was added into the solution, which was then stirred at 60 °C for 4 h. After reaction, the solution was placed in a glass petri dish, immersed in water for regeneration, and hot-pressing for drying to obtain RC/P/ZnO composite antibacterial film.

Density of the films

The film was cut as a square with the size of 2×2 cm, its thickness was 0.01 cm, weight was 0.0324 g, and its density was calculated as 0.811 g/cm^3.

Characterization

Figure 1 provides a mechanistic view of the formation of a composite film, along with the steps involving crosslinking of the mixture including RC and PZnO.

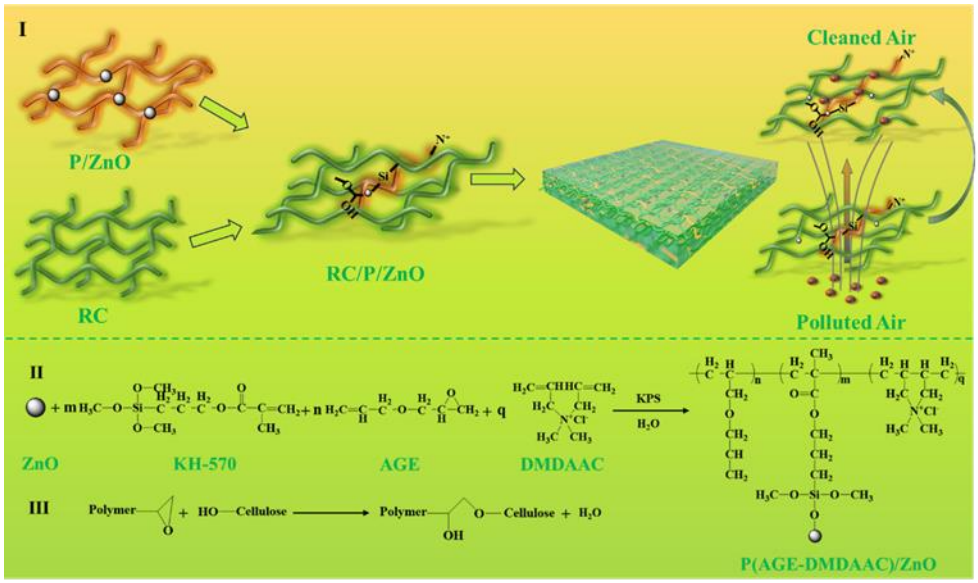

Fig. 1. Mechanistic diagram of composite film formation, process flowchart for RC and P/ZnO cross-linked composite film preparation: Particle filtration diagram (I), Synthetic mechanism diagram for P/ZnO (II), and Cross-linking mechanism diagram for P/ZnO and cellulose (III)

The morphologies of the film samples were measured using a Nova Nano Sem 450 (FEI, Hillsboro, OR, USA) scanning electron microscope (SEM) at an accelerating voltage of 5.0 kV. Additionally, energy-dispersive spectroscopy (EDS) was employed to determine the elemental composition of both RC and the composite antibacterial film.

Chemical composition of films were obtained using a Fourier transform infrared (FTIR) spectrometer (Nicolet 560, Bruker, Billerica, MA, USA), in the range of 400 to 4000 cm^{-1}. The spectral resolution was set at 1.0 cm^{-1}.

Thermogravimetric analysis (TGA) was carried out using a Netsch sta-449e (Netsch, Germany) device. 5 mg sample powder was added to a 70 µL alumina crucible. A test was conducted in a nitrogen atmosphere, from 20 to 800 ℃, and the heating rate was 10 ℃/min. Using TA Instruments DSC-2910 Modulated DSC under N_2 protection, the sample of about 7 mg was changed from room temperature to 800 ℃/min at 25 ℃/min and kept constant for 5 min. The material was scanned to room temperature at a cooling rate of 10 ℃ /min and analyzed.

Tensile tests were conducted in stretch mode using a universal testing machine (TSE103A, Shenzhen, China). The tensile tester was equipped with a 1000 N load cell, and the tensile speed was adjusted to 1 mm/min during the test. The composite film was cut into a long strip with a width of 15 mm and a thickness of 0.2 mm. Each sample was measured 3 times and the average value was taken.

A particle counter (DT-9881, CEM, America was used to measure particulate matter concentration (PM). Air containing particles ($PM_{0.3}$, $PM_{0.5}$, $PM_{1.0}$, $PM_{2.5}$, $PM_{5.0}$, and $PM_{10.0}$) were introduced into the filtration setup at a flow rate of 5.3 $cm.s^{-1}$. After comparing the PMx concentrations before filtration (C_{in}, $\mu g/m^3$) and after filtration (C_{out}, $\mu g/m^3$), the PMx filtration efficiency (η) was calculated,

$$\eta = (C_{in} - C_{out}) / C_{in} \quad (1)$$

$$\Delta P = P_{in} - P_{out} \quad (2)$$

where P_{in} is pressure measurements before filtration (Pa), P_{out} is pressure measurements after filtration (Pa), and ΔP is the filtration resistance (Pa).

Antibacterial Activity

About 100 µL volumes of *E. coli* (Gram-negative bacterium) and *S. aureus* (Gram-positive bacterium) were used and added separately to RC films, RC/P films, and RC/P/ZnO films. The samples were incubated at 37 °C for 18 h, and then rinsed with 10 mL sterile water. The rinsed bacterial suspension of 100 µL was coated on the AGAR plate and cultured again at 37 °C for 12 h for colony counting.

RESULTS AND DISCUSSION

Dissolution Characteristics

The morphologies of cellulose solution samples are displayed in Figs. 2a through 2e. Undissolved fibre-like structures still remained in the solution when the concentration of LiCl was below 6% (Abbasi Moud *et al*. 2021). In contrast, no filler-like structures were observed in cellulose solutions when the usage of LiCl were over 6%, suggesting that the cellulose molecules were well dissolved. According to the economic benefit and dissolution, the usage of LiCl was chosen as 6% in the further experiment. In addition, both dissolved solutions under 2% and 4% cellulose concentrations exhibited excellent flow properties (Fig. 2f), indicating that these solutions have prominent processability. Compared with other cellulose solutions, the dissolution efficiency of 4% cellulose was

higher; hence, the dissolution conditions were chosen as 6% LiCl and 4% cellulose for further experiments.

SEM Analysis

The morphologies of RC and P/ZnO composites are shown in Figs. 2j and 2k. Because of the cross-linking of propylene oxide with cellulose, the composited film surface exhibited network-like structures. The P/ZnO composites were coated on the surface of RC or were present among them. It was worth noting that ZnO can still be observed in composite materials after water cleaning. It was apparent that the ZnO was stable in the composite material through Si-O bonding (Zhang *et al*. 2019b). In addition, the result of EDS exhibited that nitrogen (N) and zinc (Zn) elements were uniformly distributed on the surface of RC/P/ZnO (Figs. 2g, 2h, and 2i). It was further shown that P/ZnO was successfully cross-linked to RC.

Chemical Structure Characterization

The FTIR spectroscopy characterized the chemical structures of RC, P(AGE-DMDAAC), P/ZnO, and RC/P/ZnO, as shown in Fig. 3a. The peaks at 2900, 1314, and 1130 cm^{-1} were the stretching vibrations of C-H and the C−O−C groups (Ahne *et al*. 2018). Moreover, the emergence of Si-O-Zn peaks at 990 cm^{-1} and Zn-O peaks at 476 cm^{-1} indicates the effective grafting of nano ZnO onto P/ZnO (Pan *et al*. 2019).

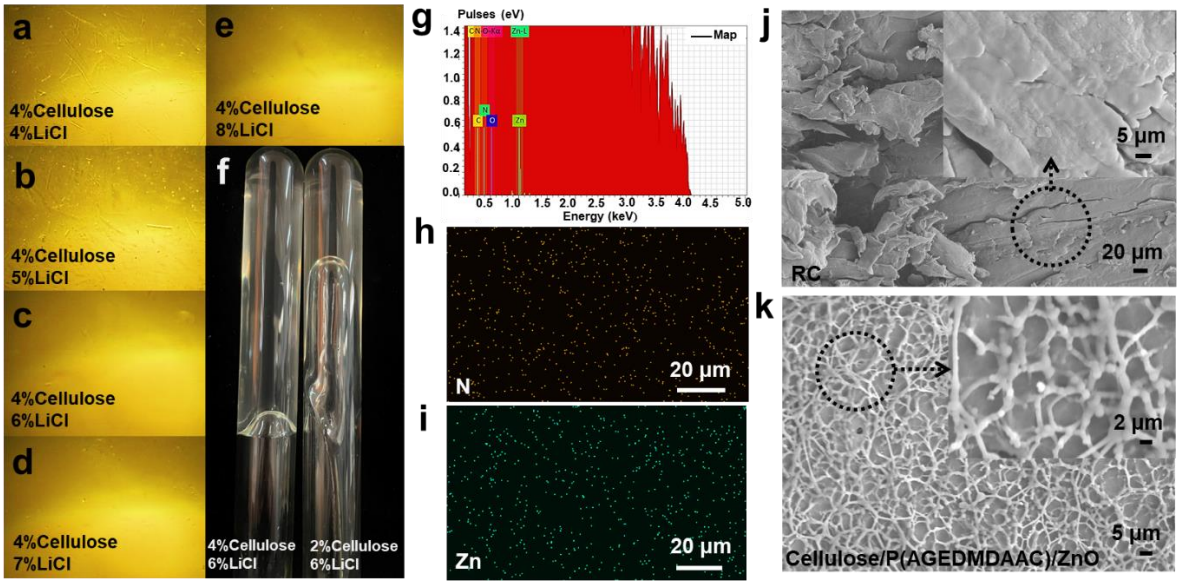

Fig. 2. Microscopic images of cellulose solutions at different LiCl concentrations **a** to **e**; flow behaviour of cellulose solutions at different cellulose concentrations **f**; EDS spectroscopy **g**-**i** and SEM images of RC and composite antibacterial films **j**, **k**

A hydroxyl stretching absorption peak of cellulose was observed at 3430 cm^{-1}, while the peak was slightly red-shifted (at 3460 cm^{-1}) in RC/P and RC/P/ZnO. This demonstrated the reduction of the amount of hydrogen bonds, indicating that more hydroxyls had reacted with P/ZnO, and the amount of hydrogen bonds was reduced. Meanwhile, the spectral bands from 890 cm^{-1} were assigned to stretching and deformation vibrations characteristic of C−O−C bond, which indicated that P(AGE-DMDAAC) was

successfully prepared (Abbasi Moud *et al*. 2021). The peaks at 990 cm^{-1} were assigned to Si−O−Zn, and that at 476 cm^{-1} was for Zn−O vibrations. These findings indicated that the nano ZnO was grafted to KH570. All this evidence showed that RC/P/ZnO was successfully prepared in this study.

The crystallinity of RC and RC/P/ZnO film were measured by X-ray diffraction, and their spectrograms are displayed in Fig. 3b. The diffractograms of both films were appraised by a main diffraction peak near 20° (Brzyski *et al*. 2019). The results indicated that the cellulose was primarily constituted as the cellulose-II crystal type. The XRD curve of P/ZnO showed peaks at 34.4° and 36.2°, corresponding to diffraction in the ZnO (002) and (101) planes (Elfeky *et al*. 2020). In addition, P(AGE-DMDAAC) was complexed with nano-ZnO, resulting in changes in its crystal lattice, so P/ZnO rarely appeared as diffraction peaks at 25° and 61°. All the evidence showed that the sample was mainly composed of cellulose-II.

Thermogravimetric Analysis

To evaluate the hydrogel thermal stability of RC, P(AGE-DMDAAC), P/ZnO, and RC/P/ZnO, TGA analysis was performed. Results are shown in Fig. 3c. Because of the evaporation of free and bound water, a minor weight loss was noticed below 220 °C from all these samples (Liu *et al*. 2013). In the range of 250 to 370 ℃, the composites underwent the first stage of thermal degradation, during which the glucoside bond of the cellulose chain was broken and carbon dioxide and other hydrocarbon derivatives were produced. Meanwhile, the polymerization degree was reduced. The weight loss in this region can be attributed to the thermal decomposition of P(AGE-DMDAAC), which involved the breaking of the C-N, C-O, and C=O bonds in the side chain. Subsequently, in the range of 410 to 480 °C, the C-C bonds in the main chain broke (Nemoto *et al*. 2012). Notably, the degradation temperature of P in the second stage was higher than that of P/ZnO, primarily due to the high rupture temperature of the Si-O-CH_3 bond. In addition, Fig. 3d shows that the maximum decomposition temperature (T_{max}) of RC/P/ZnO was 375 °C, which was higher than that of RC film (350 °C). The residual inorganic substance levels of P (13.8%), and P/ZnO (15.3%) were lower than those of RC and the composite materials. The residual mass of RC/P/ZnO after decomposition was 19.9%, which was more than that of RC films. In Fig 3e, two peaks of the polymer appeared, with an initial temperature of 25 °C and a cold crystallization peak at a maximum temperature of 100 °C. The initial temperature of the second peak was 230 ℃, and the maximum temperature was 310 ℃, resulting from the double bond polymerization of monomer. After ZnO was added, the second melting peak moved towards low temperature. The interaction between ZnO and polymer molecular chains is complex, which limits the movement of polymer molecular chains and reduces the thermostability temperature of grains. After ZnO was added, the curing heat increased from 408.6 to 582.8 J/g, and the higher of the ΔH was, the more complete the curing reaction per unit time was observed. The addition of polymer has no significant effect on the thermostability, and the melting temperature was about 300 ℃. When the polymer was added, the curing heat increased from -91.27 to -69.14 J/g, and the curing reaction was more complete. Zinc oxide nanoparticles (ZnO NPs) and curcumin were further added to RC (Raha and Ahmaruzzaman 2022). Weight loss occurred at 250 to 400 °C. T_{onset} and T_{max} had a higher microcrystalline cellulose (303 and 339 °C) contents than the extracted cellulose (286 and 336 °C). The presence of P/ZnO obviously reduced the residue of RC. The thermostability of the composite materials was slightly higher than that of RC, indicating the addition of P/ZnO was took advantage on their thermostability.

Mechanical Characteristics

To investigate the mechanical properties of RC and composited materials, the tensile stress and Young's modulus were tested. The tensile strength and Young's modulus of chemical-crosslinking RC/P/ZnO (206.8 MPa and 4.3 GPa) films were obviously higher than those of RC film (23.7 and 350 MPa) (Figs. 4a and 4b). Results indicated that the mechanical properties of materials were enhanced sharply by the P/ZnO introduction. On the one hand, the P/ZnO network-like structures increased the value of crosslinking in RC film and provide more supporting points to resist the stretch stress (Jiang *et al*. 2020). On the other hand, friction among polymer chains can be enhanced and can restrict the movement of the chains by introducing P/ZnO into RC film, resulting in strain reduction. It was evidenced that the incorporation of ZnO further elevated the stress and Young's modulus of RC composited material. This noteworthy enhancement of mechanical properties was elucidated by the effective transmission of stress between RC and ZnO components, facilitated by robust interfacial adhesion and interactions. Mir *et al*. (2016) blended water-soluble sodium carboxymethylcellulose with high-density polyethylene. The maximum tensile strength of the cross-linked blend was 19.6 MPa. The tensile strength and Young's modulus of composited films was 8.7 and 12.2 times than that of RC films, respectively. According to this evidence, the mechanical properties of RC composited film was strong enough for application in various environments.

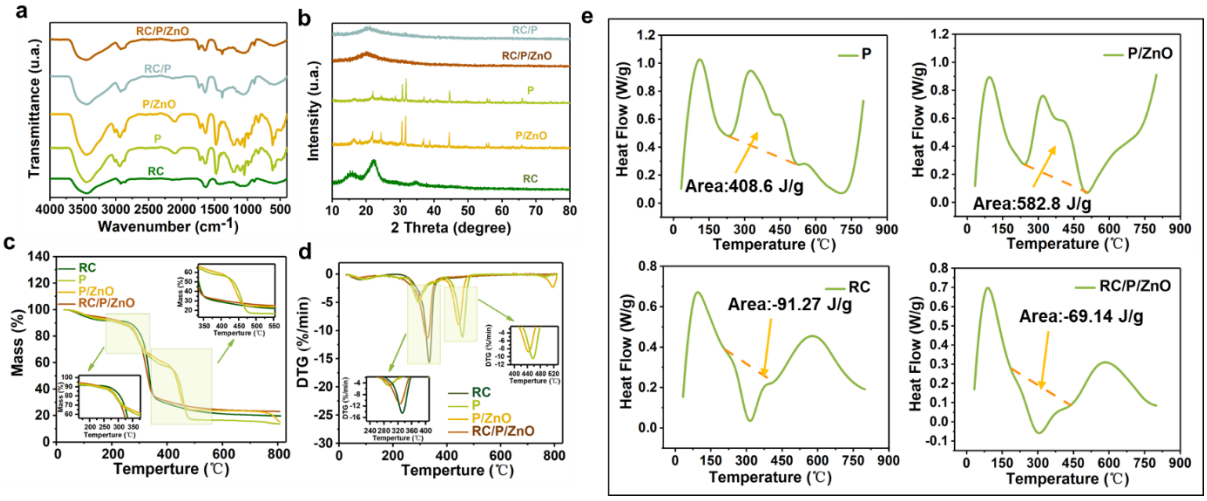

Fig. 3. Chemical structure and morphological analyses of polymer and composite antibacterial films: FTIR spectra of RC, polymer, and composite antibacterial films **a**; XRD patterns **b**; thermogravimetric analysis (TGA) **c**; Differential thermogravimetric analysis (DTG) **d**; Differential scanning calorimetry (DSC) **e**

Filtering Performance

The authors employed non-oily PMx particles, which are created by burning incense in this process. The FE reached up to 98.81%, 98.90%, 98.93%, 99.91%, 99.96%, and 99.97% for nonoily PMx for $PM_{0.3}$, $PM_{0.5}$, $PM_{1.0}$, $PM_{2.5}$, and $PM_{5.0}$, respectively (Figs. 4c and 4d). For particles in the range of 0.1 to 1.0 μm, the main trapping mechanism is interception. Therefore, this study showed a small FE in tiny PMx ($d \leqslant 1.0$ μm) (Liu *et al*. 2021). For particles larger than 1.0 μm, inertial deposition is the most common trapping method. In this study, for PMx ($d > 1.0$ μm), the two trapping mechanisms function simultaneously, and the FE is larger. The addition of more P/ZnO enhanced the film's FE.

The network structure of cellulose enables small particles to pass through the membrane. However, the addition of P/ZnO makes the network structure denser, increasing its specific surface area and porosity (Wang *et al*. 2019). Therefore, the addition of P/ZnO improved the interception and inertial deposition effect of RC film, and more efficiently removed airborne particles.

Hydrophobic Property

To evaluate the hydrophobic properties of composited films, the submerging bath method was employed, RC film was used as control (Fig. 4e). Notably, the composited film still floated on the surface of DI water even after 7 days, The unexposed side of the RC/P/ZnO film remained impermeable to moisture, in contrast to the RC film, which absorbed water and eventually became submerged. Results showed the pivotal role of Si-O from polymer synthesis in P/ZnO, which imparts exceptional hydrophobic properties to the composite film. The inherent hydrophobicity of the silane group empowers KH570 to establish a defensive layer imbued with hydrophobic characteristics upon interfacing with the material surface (Liu *et al*. 2021). Concurrently, the chemical interaction between the silane group and the surface of RC enhanced the adhesive potency of silane coupling agent, thereby amplifying its hydrophobic attributes. In this study, KH570 dosage of 2.5% resulted in excellent hydrophobic properties of the composite film and a lower dosage of silanes coupling agent compared to other studies.

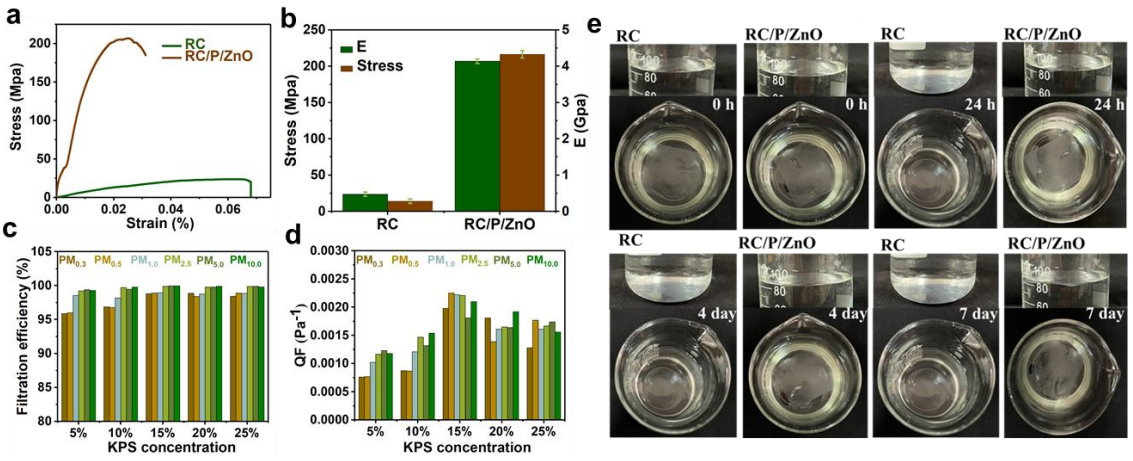

Fig. 4. Mechanical performance and filtration efficiency of RC and composite films **a** through **d**, Hydrophobicity assessment ((1) RC film, (2) RC/P film, (3) RC/P/ZnO film **e**)

Antibacterial Performance

The antibacterial activities of RC/P and RC/P/ZnO composite films against *E. coli* and *S. aureus* were studied, and results are shown in Fig. 5. The antibacterial rate of *E. coli* and *S. aureus* were more than 99%. The epoxy group in P/ZnO formed a chemical covalent bond with the hydroxyl group of the fibre, and the P/ZnO contained quaternary ammonium salt and ZnO. The inhibitory MIC values of ZnO against *E. coli* and *S. aureus* were 5 and 15 μg /mL, respectively. The antibacterial activity of ZnO against Gram-positive and Gram-negative bacteria was measured as control, as shown in Figs.5c and 5f. This experiment confirmed that electrostatic adsorption was the main antibacterial mechanism, by interaction destroys the integrity of the cell film. The surface charges of *S. aureus* were more negative in contrast to *E. coli* due to the difference in their structure and components,

necessitating the application of higher ZnO concentrations to achieve comparable antibacterial ability (Gao *et al*. 2022). Results exhibited that RC/P/ZnO composite film was effective for eliminating biofilms and exterminate bacteria. Thus, it could be regarded as an excellent antibacterial packaging material.

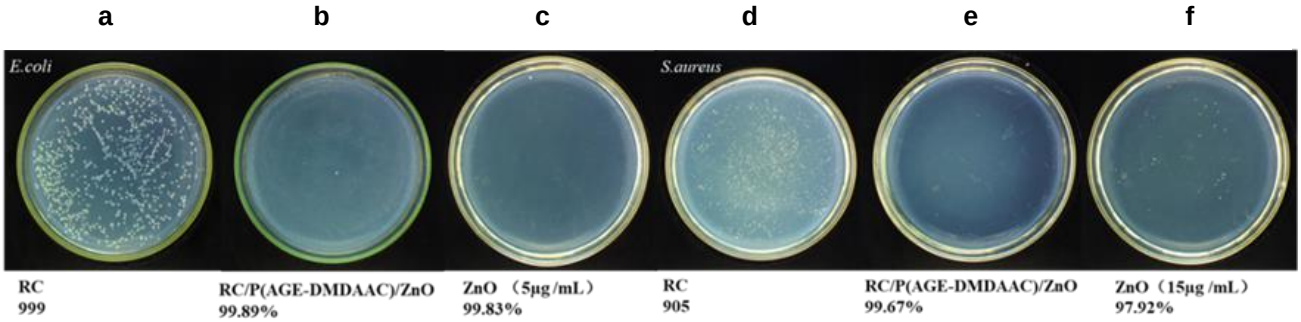

Fig. 5. Antibacterial rate of RC **a**, RC/P/ZnO **b**, and ZnO **c** against *E. coli.* Antibacterial rate of RC **d**, RC/P/ZnO **e**, and ZnO **f** against *S. aureus*

CONCLUSIONS

1. The incorporation of P/ZnO imparted the composite films with a well-defined network structure, leading to the enhancement of filtration efficiency and a substantial increase in Young's modulus.
2. The composite films exhibited strong antibacterial activity against both *E. coli* and *S. aureus* (99.89% and 99.67%, respectively).
3. The hydrophobic properties of RC composite films were improved due to the incorporation of Si-O addition. Hence, their environmental adaptability was also improved.

ACKNOWLEDGMENTS

This study was financially supported by the National Natural Science Foundation of China (52263011, 51963012), Xingdian Talent Support Program of Yunnan (YNWR-QNBJ-2020-039, YNWR-QNBJ-2020-045), and Yunnan Provincial Research Foundation for Basic Research, China (No. 202201AT070075).

REFERENCES CITED

Abbasi Moud, A., Sanati-Nezhad, A., and Hejazi, S. H. (2021). "Confocal analysis of cellulose nanocrystal (CNC) based hydrogels and suspensions," *Cellulose* 28(16), 10259-10276. DOI: 10.1007/s10570-021-04164-3

Ahne, J., Li, Q., Croiset, E., and Tan, Z. (2018). "Electrospun cellulose acetate nanofibers for airborne nanoparticle filtration," *Textile Research Journal* 89(15), 3137-3149. DOI: 10.1177/0040517518807440

Brzyski, P., Kosiński, P., Skoratko, A., and Motacki, W. (2019). "Thermal properties of cellulose fiber as insulation material in a loose state," in: *Central European Symposium on Thermophysics* 2133, Article ID 5120136. DOI: 10.1063/1.5120136

Candan, Z., Tozluoglu, A., Gonultas, O., Yildirim, M., Fidan, H., Alma, M. H., and Salan, T. (2022). "Nanocellulose: Sustainable biomaterial for developing novel adhesives and composites," *Industrial Applications of Nanocellulose and Its Nanocomposites* 2022, 49-137. DOI: 10.1016/B978-0-323-89909-3.00015-8

Elfeky, A. S., Salem, S. S., Elzaref, A. S., Owda, M. E., Eladawy, H. A., Saeed, A. M., Awad, M. A., Abou-Zeid, R. E., and Fouda, A. (2020). "Multifunctional cellulose nanocrystal /metal oxide hybrid, photo-degradation, antibacterial and larvicidal activities," *Carbohydrate Polymers* 230, article ID 115711. DOI: 10.1016/j.carbpol.2019.115711

Gao, X., Yu, Z., Tang, X., Zhang, H., Peng, L., and Li, J. (2022). "Augmented antibacterial mechanism of ZnO nanoparticles by labyrinthian-channel configuration of maize-stalk carbohydrate columns and sustainable strategy for water decontamination," *Journal of Hazardous Materials* 436, article ID 129528. DOI: 10.1016/j.jhazmat.2022.129258

Hartikainen, T., Ruuskanen, J., and Martikainen, P. J. (2001). "Carbon disulfide and hydrogen sulfide removal with a peat biofilter," *Journal of the Air & Waste Management Association* 51(3), 387-392. DOI: 10.1080/10473289.2001.10464275

Holdsworth, S. R., and Law, C. J. (2012). "The major facilitator superfamily transporter MdtM contributes to the intrinsic resistance of *Escherichia coli* to quaternary ammonium compounds," *Journal of Antimicrobial Chemotherapy* 68(4), 831-839. DOI: 10.1093/jac/dks491

Jiang, S., Lin, K., and Cai, M. (2020). "ZnO nanomaterials: Current advancements in antibacterial mechanisms and applications," *Frontiers in Chemistry* 8, article ID 580. DOI: 10.3389/fchem.2020.00580

Liu, Q., Xia, N., Wan, W., Gao, Y., and Zhu, S. (2021). "Selective capture of toxic anionic dyes of a novel prepared DMDAAC-grafted chitosan/genipin/cellulose hydrogel beads with antibacterial activity," *International Journal of Biological Macromolecules* 189, 722-733. DOI: 10.1016/j.ijbiomac.2021.08.116

Liu, Y., Ma, K., Li, R., Ren, X., and Huang, T. S. (2013). "Antibacterial cotton treated with N-halamine and quaternary ammonium salt," *Cellulose* 20(6), 3123-3130. DOI: 10.1007/s10570-013-0056-7

Nemoto, J., Soyama, T., Saito, T., and Isogai, A. (2012). "Nanoporous networks prepared by simple air drying of aqueous TEMPO-oxidized cellulose nanofibril dispersions," *Biomacromolecules* 13(3), 943-946. DOI: 10.1021/bm300041k

Pan, Z., Liang, Y., Tang, M., Sun, Z., Hu, J., and Wang, J. (2019). "Simulation of performance of fibrous filter media composed of cellulose and synthetic fibers," *Cellulose* 26(12), 7051-7065. DOI: 10.1007/s10570-019-02605-8

Poyraz, B., Tozluoglu, A., Candan, Z., and Demir, A. (2017). "Matrix impact on the mechanical, thermal and electrical properties of microfluidized nanofibrillated cellulose composites," *Journal of Polymer Engineering* 37(9), 921-931. DOI: 10.1515/polyeng-2017-0022

Raha, S., and Ahmaruzzaman, M. (2022). "ZnO nanostructured materials and their potential applications: Progress, challenges and perspectives," *Nanoscale Advances* 4(8), 1868-1925. DOI: 10.1039/d1na00880c

Ren, X., Kou, L., Liang, J., Worley, S. D., Tzou, Y.-M., and Huang, T.S. (2008). "Antimicrobial efficacy and light stability of N-halamine siloxanes bound to cotton," *Cellulose* 15(4), 593-598. DOI: 10.1007/s10570-008-9205-9

Salama, A., Abouzeid, R. E., Owda, M. E., Cruz-Maya, I., and Guarino, V. (2021). "Cellulose-silver composites materials: Preparation and applications," *Biomolecules* 11(11). article ID 1684. DOI: 10.3390/biom11111684

Shatkin, J. A., Wegner, T. H., Bilek, E. M., and Cowie, J. (2014). "Market projections of cellulose nanomaterial-enabled products. Part 1: Applications," *TAPPI Journal* 13(5), 9-16. DOI: 10.32964/tj13.5.9

Wang, B., Sun, Z., Sun, Q., Wang, J., Du, Z., Li, C., and Li, X. (2019). "The preparation of bifunctional electrospun air filtration membranes by introducing attapulgite for the efficient capturing of ultrafine PMs and hazardous heavy metal ions," *Environmental Pollution* 249, 851-859. DOI: 10.1016/j.envpol.2019.03.122

Zhu, M., Han, J., Wang, F., Shao, W., Xiong, R., Zhang, Q., Pan, H., Yang, Y., Samal, S. K., Zhang, F., *et al.* (2017). "Electrospun nanofibers membranes for effective air filtration," *Macromolecular Materials and Engineering* 302(1), article ID 353. DOI: 10.1002/mame.201600353

Article submitted: November 13, 2023; Peer review completed: December 20, 2023; Revised version received and accepted: January 13, 2024; Published: February 12, 2024.
DOI: 10.15376/biores.19.2.2149-2159